



Eidgenössische Technische Hochschule Zürich  
Swiss Federal Institute of Technology Zurich



# **Synthetic validation of a non-linear 2D-3D registration algorithm using in vivo micro-CT mouse data**

Semester Thesis

Ketan Gupta

June 5, 2023

Supervisor: Prof. Dr. Ralph Müller

Advisor: Francisco Correia Marques

Department of Health Sciences and Technology, ETH Zürich



SEMESTER PROJECT  
D-ITET, FS 2023  
Ketan GuptaSYNTHETIC VALIDATION OF A NON-LINEAR 2D-3D REGISTRATION ALGORITHM  
USING IN VIVO MICRO-CT MOUSE DATA

## 1. INTRODUCTION

Metabolic processes taking place in bone usually span multiple spatial scales, from the molecular, to cellular, tissue and on to the organ level. Therefore, unravelling the underlying mechanisms governing bone adaptation and regeneration requires a multiscale approach that connects organ and tissue-level analysis with the (sub-)cellular scale. While the former two are well-established in the field through micro-finite element (micro-FE) simulations or static and dynamic morphometry analysis of bone structure, the latter has seen modest improvements.

In this regard, a Local *in vivo* Environment (LiVE) imaging pipeline has been developed in our group [1], combining *in vivo* micro-computed tomography (micro-CT) imaging, micro-FE analysis and histological analysis to relate cell-scale activity to tissue-level mechanical properties. Specifically, 2D immunohistochemistry slices allow estimating the expression of biomarkers (e.g., RANKL and Sclerostin) by osteocytes which are also mapped to their 3D location on the micro-CT scan of the bone structure. The same 3D model is used to compute the mechanical signals in the structure using micro-FE. Furthermore, by leveraging longitudinal micro-CT imaging, cell protein expression can even be linked to regions of bone formation and bone resorption. Indeed, promising results have suggested a link between resorption surfaces with higher RANKL expression and low local mechanical strain values compared to formation surfaces exhibiting high mechanical strains, indicating that the local mechanical environment also regulates bone remodelling [2].

Nevertheless, an accurate and validated multi-modality registration is crucial to achieve meaningful results. To this end, synthetic datasets can be generated from a single modality (here, the binarized 3D micro-CT image) with known ground truth that can be compared with the output of the registration. In particular, given that sectioning of histological sections can introduce non-linear deformations in the 2D structural images, recreating those conditions *in silico* and investigating how such deformations interfere with the registration step can provide valuable insights to develop more robust registration algorithms. Likewise, datasets with increasing levels of deformations can be efficiently created, enabling a thorough identification and characterisation of the most influential deformations on the registration step.

First, synthetic datasets of 2D images with non-linear deformations will be generated for samples from an existing mouse femur dataset. Next, *in silico* simulations will be performed to register those synthetic 2D images to the corresponding 3D volume. A non-linear registration step will follow the affine phase and attempt to recover the original 2D image. Finally, the accuracy and the convergence of the registration will be quantified, as a function of the deformation level applied to the initial undeformed image.

## 2. RESOURCES REQUIRED

- Computer (ISG D-HEST) and desk in student room (HCP/H24.2 or H15.2)
- Access to the Gitlab framework
- Access to Malleus for software development, data analysis and visualisations
- Access to Euler for model development

### 3. TASK LIST

- Write a detailed timetable of the work to be performed
- Review the literature relevant to multi-modal 2D-3D registration
- Implement appropriate metrics to assess the sensitivity of 2D-3D registration
- Generate ground-truth 2D data from 3D micro-CT images
- Perform 2D-3D registration of the generated data
- Perform a statistical analysis of the performance metrics collected
- Write a detailed report of the project
- Present the work in a final presentation of 20 minutes

### 4. LITERATURE

- [1] A. J. Trüssel, "Spatial mapping and high throughput microfluidic gene expression analysis of osteocytes in mechanically controlled bone remodeling," no. 22716, 2015.
- [2] A. C. Scheuren *et al.*, "Mechano-regulation of trabecular bone adaptation is controlled by the local in vivo environment and logarithmically dependent on loading frequency," *Front. Bioeng. Biotechnol.*, vol. 8, p. 1211, 2020, doi: 10.3389/FBIOE.2020.566346.
- [3] E. L. Lundin *et al.*, "Automatic registration of 2D histological sections to 3D microCT volumes: Trabecular bone," *Bone*, vol. 105, pp. 173–183, 2017, doi: 10.1016/j.bone.2017.08.021.
- [4] O. Museyko *et al.*, "Registration of 2D histological sections with 3D micro-CT datasets from small animal vertebrae and tibiae," *Comput. Methods Biomed. Engin.*, vol. 18, no. 15, pp. 1658–1673, 2015, doi: 10.1080/10255842.2014.941824.

Student Project, FS 2023

Start of Project: 27.02.2023  
End of Project: 05.06.2023

Project Supervisor:

(Signature/Date):

Ralph Müller  
2023.02.16 18:12:21 +01'00'

Prof. Ralph Müller  
Institute for Biomechanics, D-HEST

Project Advisor:

Francisco Correia Marques  
Email: [francisco.correia@hest.ethz.ch](mailto:francisco.correia@hest.ethz.ch)  
Telephone: +41 44 633 91 22

---

## Abstract

This project sought to evaluate the effects of deformations of 2D synthetic histological slices and positional initializations on the 2D-3D registration algorithm developed by the Lab for Bone Biomechanics. Synthetic 2D histological slices were sampled from 3D micro-CT images of mouse femurs with different bone volume over total volumes. It was found that with higher degrees of deformation, the registration algorithm would converge less frequently and with a greater error. The same was seen when the rotational and translational initializations prior to beginning the registration were further away from their respective ground truth values. Additionally, it was found that sampling a 3D micro-CT bone image further away from its center had no bearing on the registration error regardless of deformation of the synthetic 2D slice.

---

## Acknowledgement

I would like to thank Prof. Dr. Müller for the opportunity to pursue a project with his research group at D-HEST and learn about the fascinating process of image registration. I relished the experience and it helped me build my programming and data visualisation skills. I would also like to thank my advisor, Francisco Correia, for taking the time to teach me about the server setup as well as for his patience in explaining concepts to me. I am deeply grateful for his extensive insight and help with this project.

---

# Contents

---

<b>Contents</b>	<b>iii</b>
<b>1 Introduction</b>	<b>1</b>
<b>2 Background</b>	<b>3</b>
2.1 Linear transformations . . . . .	3
2.2 Cost functions . . . . .	5
2.2.1 Euclidean distance transform (EDT) . . . . .	5
2.2.2 EDT Pearson's correlation coefficient (EDTPe) . . . . .	6
2.2.3 Normalized mutual information (nMI and EDTnMI) . . . . .	6
2.2.4 Dice similarity coefficient of the surface (DS) . . . . .	7
2.3 Powell's method for optimization . . . . .	8
2.4 Previous attempt by the group . . . . .	9
<b>3 Materials and Methods</b>	<b>11</b>
3.1 Generation of synthetic datasets . . . . .	11
3.2 Registration algorithm . . . . .	12
3.2.1 Initial guess . . . . .	13
3.2.2 Cost functions . . . . .	13
<b>4 Results and Discussion</b>	<b>15</b>
4.1 Generation of synthetic slices . . . . .	15
4.2 Evaluation of initialization and deformation on registration results . . . . .	17
4.2.1 Successful convergence of the Powell optimizer . . . . .	17
4.2.2 Accuracy of the Powell optimizer . . . . .	23
4.2.3 Effect of displacement $ dx_{gt} $ on DRE . . . . .	29
<b>5 Conclusion</b>	<b>33</b>
<b>Bibliography</b>	<b>35</b>



## Chapter 1

---

# Introduction

---

The Lab for Bone Biomechanics is working on revealing the underlying mechanisms that govern bone adaptation and regeneration. These processes of bone metabolism must be studied at different scales, from organ and tissue to the cellular. While the former two have been extensively studied through micro-finite element simulations, there exists a need to connect them to cellular phenomena. To this end, the group has developed a Local in vivo Environment (LivE) imaging pipeline [1].

This pipeline combines in vivo micro-computed tomography (micro-CT) imaging with histological analysis to relate cell-scale activity to tissue-level mechanical properties of bone. The 2D immunohistochemistry slices allow estimation of the expression of various biomarkers by osteocytes. Such slices can be mapped to their 3D location on their respective micro-CT images via registration. Promising results have suggested a link between resorption surfaces with higher RANKL expression and low local mechanical strain values compared to formation surfaces exhibiting high mechanical strains, indicating that the local mechanical environment also regulates bone remodeling [2].

In view of achieving meaningful results in future studies, it is essential that accurate, validated and multi-modal registration methods be developed. In order to do this, synthetic datasets for 2D histological slices can be generated from a single modality (binarized 3D micro-CT image in this case). Such datasets - with known ground truths - can be compared with the output of the registration algorithm. It must be noted that sectioning of histological slices can cause deformations in the tissue being examined. In order to simulate this, varying degrees of deformation can be added to the synthetic dataset. This will help examine how deformation may interfere with the registration, which may help develop more robust algorithms in the future.

## 1. INTRODUCTION

---

The aims for the project were as follows:

1. Generate synthetic datasets with increasing levels of deformation from longitudinal micro-CT mouse femur images with four different values of bone volume over total volume (BV/TV)
2. Perform 2D-3D registration of the simulated slices onto their respective micro-CT images
3. Visualise the results and effects of several parameters on the registration

## Chapter 2

---

# Background

---

Image registration is the process of transforming an image in a “source” coordinate space to a “target” coordinate space. This is often required when aligning images that have been captured with different imaging parameters such as angle, illumination or times. Registration is a key component of many applications involving image analysis. An example of this is in time-lapsed micro-CT imaging. Two CT images are captured one week apart. The positioning of the specimen in the scanner at these two points is not identical, and as a result the same cross-sectional slices from each of the images have slightly different anatomical features. Registration is required in order to align the two 3D images so that a valid comparison can be made in order to properly compare the tissue at the two time-points. This particular example was an intra-modality registration.

### 2.1 Linear transformations

Registration is performed via geometric transformations. For the scope of this project, the focus will be on linear transformations. These transformations are linear as they can be computed using matrix multiplication. They are of the form [3]:

$$x' = T(x) = Ax + t, \quad t = \begin{bmatrix} t_1 \\ t_2 \\ t_3 \end{bmatrix}, \quad x = \begin{bmatrix} x_1 \\ x_2 \\ x_3 \end{bmatrix} \quad (2.1)$$

Here,  $A$  is the transformation matrix and will have the shape  $3 * 3$  as the registration is 2D to 3D.  $t$  is the translation vector and will have the shape  $3 * 1$ .  $x$  denotes the coordinate space of the 2D histological slice and  $x'$  denotes the coordinate space of the 3D micro-CT femur image.  $x_1$ ,  $x_2$  and  $x_3$  are unit vectors along the x, y and z axes respectively.

## 2. BACKGROUND

---

Linear transformations can fall into three categories:

- Rigid body
- Similarity
- Affine

Rigid body transformations are when an image is rotated or translated. The objects in the image do not undergo any change in shape or size. In 2 dimensions, if the angle of rotation is  $\theta$  [3]:

$$x' = T(x) = Rx + t, \quad R = \begin{bmatrix} \cos(\theta) & -\sin(\theta) \\ \sin(\theta) & \cos(\theta) \end{bmatrix} \quad (2.2)$$

In 3 dimensions, the rotation matrix  $R$  is parameterized with three angles.  $\varphi$  = rotation about the z-axis,  $\theta$  = rotation about the y-axis and  $\psi$  = rotation about the x-axis. The number of parameters is 6 (3 for rotation + 3 for translation) [3]. It must be noted that in 3D, the order of image rotations matters i.e.  $R(\varphi)R(\theta) \neq R(\theta)R(\varphi)$  [3].

$$R = R(\varphi)R(\theta)R(\psi) \quad (2.3)$$

$$R(\varphi) = \begin{bmatrix} \cos(\varphi) & -\sin(\varphi) & 0 \\ \sin(\varphi) & \cos(\varphi) & 0 \\ 0 & 0 & 1 \end{bmatrix} \quad (2.4)$$

$$R(\theta) = \begin{bmatrix} \cos(\theta) & 0 & -\sin(\theta) \\ 0 & 1 & 0 \\ -\sin(\theta) & 0 & \cos(\theta) \end{bmatrix} \quad (2.5)$$

$$R(\psi) = \begin{bmatrix} 0 & 0 & 1 \\ 0 & \cos(\psi) & -\sin(\psi) \\ 0 & \sin(\psi) & \cos(\psi) \end{bmatrix} \quad (2.6)$$

Similarity transformations have the same operations as rigid body transformations, as well as isotropic scaling [3]. For similarity transformations, the entries along the diagonal of the scaling matrix  $S$  (Eq. 2.7) are the same i.e.  $s_1 = s_2 = s_3 = s$ . This scaling is isotropic and zooms in or out of the image with the scaling factor  $s$ ; the shape of the objects is preserved. If any of the values are different, then the scaling is anisotropic and the operation is no longer a similarity transformation. Anisotropic scaling in 3D requires 9 parameters (3 rotation + 3 scaling factors + 3 translation) [3].

$$x' = T(x) = RSx + t, \quad S = \begin{bmatrix} s_1 & 0 & 0 \\ 0 & s_2 & 0 \\ 0 & 0 & s_3 \end{bmatrix} \quad (2.7)$$

Affine transformations extend anisotropic scaling with a shear matrix  $W$  [3]. Shearing is when the image is stretched along a chosen direction.

$$x' = T(x) = WRSx + t, \quad W = \begin{bmatrix} 1 & w_1 & w_2 \\ 0 & 1 & w_3 \\ 0 & 0 & 1 \end{bmatrix} \quad (2.8)$$

The registration in this project uses affine transformations. The registration in 3D (to select the optimal slice from the micro-CT image) is rigid; after the 2D slice is taken, an affine registration is performed. The rigid 3D component has 6 parameters: 3 for rotation and 3 for translation [3]. The affine 2D component is an anisotropic scaling, and so requires 2 parameters for scaling along x and y. This means the registration in this project has 8 parameters. This is described further in Section 3.2.

## 2.2 Cost functions

In this project, I used image similarity metrics as the cost functions for registration. Combinations of four different similarity metrics were used: Euclidean distance transformed Pearson's correlation coefficient (EDTPe), Euclidean distance transformed normalized mutual information (EDTnMI), normalized mutual information (nMI) and Dice similarity coefficient of the surface (DS).

### 2.2.1 Euclidean distance transform (EDT)

An Euclidean distance transform can be used in an image which has a clear foreground (comprised of objects) and a background. This transform, for each pixel in the foreground, computes the closest distance to a background pixel. The result of this is a grayscale image where the intensity of a pixel denotes the closest distance of that pixel to a background pixel. Bright pixels indicate those pixels being further away from the background.

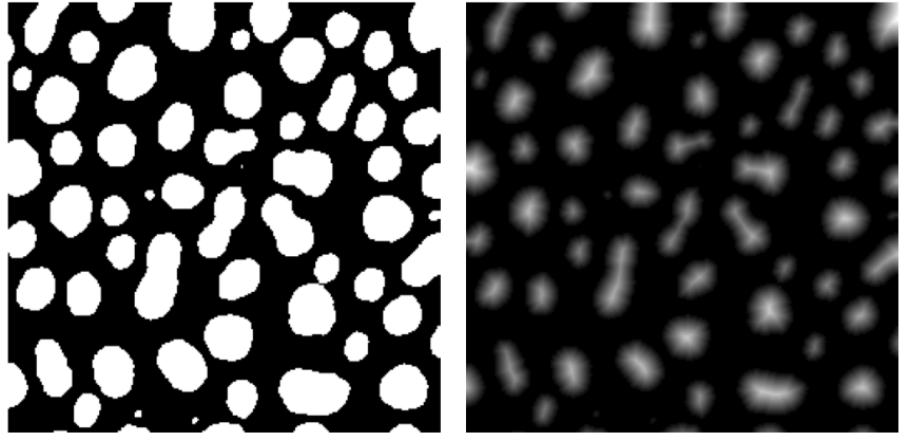


**Figure 2.1:** An illustration of the Euclidean distance transform [4]. On the left is a binary image with a white foreground and black background. On the right is the EDT of that image.

### 2.2.2 EDT Pearson's correlation coefficient (EDTPe)

Pearson's correlation coefficient is a way to compare two images to each other. It tells us the degree to which two images are linearly related to one another. If two images are linearly related, the coefficient's value will be 1. If they are completely independent, the value will be 0. Thus, when registering two images, it is desired to **maximize** the Pearson correlation coefficient. This coefficient is a way to quantify the similarity and degree of alignment between two images  $X$  and  $Y$ . It is given by  $r$  [5]:

$$r(X, Y) = \frac{\sum_{i \in \Omega} (x_i - \mu_X)(y_i - \mu_Y)}{\sqrt{\sum_{i \in \Omega} (x_i - \mu_X)^2} \sqrt{\sum_{i \in \Omega} (y_i - \mu_Y)^2}} \quad (2.9)$$

where  $\Omega$  represents the space of all pixels in  $X$  and  $Y$ ,  $x_i$  and  $y_i$  represent the intensities of each pixel in  $X$  and  $Y$  respectively and  $\mu_X$  and  $\mu_Y$  represent the mean intensities of  $X$  and  $Y$  respectively.

In this project,  $r(X, Y)$  is computed on the distance transforms of the fixed image ( $X$ : EDT of the image we want to register to) and the moving image ( $Y$ : EDT of the image we want to register).  $X$  and  $Y$  are binary images of bone tissue.

### 2.2.3 Normalized mutual information (nMI and EDTnMI)

Mutual information is another way to quantify the similarity between two images. It is defined as the Kullback-Leibler divergence ( $D_{KL}$ ) between the joint distribution of the intensities of two images and the product of the marginal distribution of the same. It is given by [6]:

$$MI(X, Y) = D_{KL}(P(I_X, I_Y) || P(I_X)P(I_Y)) = \sum_{x \in I_X} \sum_{y \in I_Y} p(x, y) \log_2 \frac{p(x, y)}{p(x)p(y)} \quad (2.10)$$

In the above equation, we can consider  $I_X$  and  $I_Y$  to be random variables that represent the intensities of two images  $X$  and  $Y$  respectively. The realizations of these random variables are  $x$  and  $y$ . Their marginal probability distributions  $P(I_X)$  and  $P(I_Y)$  are found from the normalized histograms of the respective images. The joint distribution  $P(I_X, I_Y)$  is found from the normalized joint histogram of the two images. If  $I_X$  and  $I_Y$  are completely independent from each other, the mutual information will be zero as the numerator in the log term will be 1. Perfectly aligned images will have a strong statistical relationship and MI will have a high value. Hence, the goal for registration is to **maximize** MI.

To normalize the mutual information,  $MI(X, Y)$  is multiplied by a normalization factor:

$$nMI(X, Y) = MI(X, Y) \times \frac{1}{\log_2(S_{I_X})} \quad (2.11)$$

where  $S_{I_X}$  denotes the number of possible states of  $I_X$ . In this project, the nMI is calculated for binary images of bone tissue as well as for the EDT of the same. For the binary images, the number of possible states is 2. For the EDT of the image, the number of possible states equals the number of bins in the marginal histograms.

#### 2.2.4 Dice similarity coefficient of the surface (DS)

The Dice similarity coefficient, also known as the Dice score, is a way to quantify the overlap between two segmented images. For two binary images, it is given by:

$$DS(X, Y) = \frac{N_{common}}{N_X + N_Y} \quad (2.12)$$

where  $N_{common}$  is the number of pixels of  $X$  and  $Y$  that hold the same value and  $N_X$  and  $N_Y$  are the number of pixels of  $X$  and  $Y$  respectively. For two binary images with the same pixel dimensions,  $N_{common}$  can be calculated by overlaying the images on top of each other, performing a logical AND operation on each pixel and counting the number of 1s after this. If there are no pixels in common, the Dice score is 0 as the numerator in Eq. 2.12 is 0. If the images are perfectly overlapping with each other, the Dice score will

## 2. BACKGROUND

---

be 1 since all pixels hold the same value. Therefore, for image registration, the goal is to **maximize** the Dice score.

### 2.3 Powell's method for optimization

Powell's method is a gradient-free minimization technique. If a function  $f(t)$  is to be maximized, that is the same as minimizing  $-f(t)$ . This principle can be applied to the similarity functions for image registration when using Powell's method to estimate registration parameters.

Before beginning iterations for Powell's method, some initial conditions need to be defined.

**Step 1:** An initial guess  $x^{(0)}$  for the registration parameters is provided by the user (3.2.1). If the parameter space is  $n$ -dimensional,  $n$  directions are established. The directions  $s_1, \dots, s_n$  are initialized to be the unit vectors along the respective axes. Initialize  $z^{(1)} = x^{(0)}$ . Set the main iteration counter  $k = 0$  and the cycle counter  $i = 1$ .  $i$  goes from  $1, \dots, n$ . Set the counter  $j = 0$ .

**Step 2:**

## 2.4. Previous attempt by the group

---

2.1	<p>Determine a univariate minimizer <math>\lambda_i^*</math> for the problem <math>f(z^{(i)} + \lambda_i s^{(i)})</math>.  Set <math>z^{(i+1)} = z^{(i)} + \lambda_i^* s^{(i)}</math>, and increment <math>i \leftarrow i + 1</math>.  Repeat step 2.1 until <math>i = n + 1</math>.  Check for termination (i.e. use the criterion in step 3)  Go to step 2.2a if the original version is desired, or  go to step 2.2b if the variant avoiding linearly dependent directions is chosen</p>
2.2a	<p>New direction selection (pattern search directions)  <i>(Original version of the method)</i>  Set <math>j \leftarrow j + 1</math>.  IF <math>j \leq n</math>  THEN replace <math>s^{(j)}</math> by <math>z^{(n+1)} - x^{(k)}</math>.  ELSE reset search direction set to the coordinate directions.  END IF  Set <math>x^{(k+1)} = z^{(n+1)}</math>;  initialize <math>z^{(1)} = x^{(k+1)}</math>;  increment counter <math>k \leftarrow k + 1</math>;  set <math>i = 1</math>, go to step 2.1.</p>

**Figure 2.2:** Step 2 of the Powell optimization method [7]

**Step 3:** The termination criterion is defined as:  $|z^{(n+1)} - x^{(k)}| \leq \varepsilon$ . This is to say the algorithm will terminate when the change in the similarity function between  $z^{(n+1)}$  and  $x^{(k)}$  is less than the desired accuracy  $\varepsilon$ .

The 1D minimizer in Step 2.1 evaluates the chosen similarity function(s) along a line determined by the direction  $s_i$  and chooses the point that is a local minima. This is described further in 3.2.

## 2.4 Previous attempt by the group

The group previously developed a registration algorithm that was the precursor to the one in this project. In order to initialize the parameters for Powell optimization, the old algorithm performed a random guess and chose the set of parameters with the lowest loss function. This was done by slicing the micro-CT volume into n 2500 equally spaced and rotated slices. Each of these slices was further geometrically transformed in order to find the initial

## 2. BACKGROUND

---

guess by minimizing the grayscale least square difference. The best fitting of the slices was chosen as the initial guess.

Next, this initial guess was used as the starting point of a steepest gradient descent algorithm to find the local least square difference minimum.

This project's registration algorithm differs from the precursor in two major aspects. The first is in how the registration parameters are initialized. Our algorithm does not evaluate a large number of sampling planes; it has a predefined set of initialization parameters (Subsection 3.2.1). The second is in the fact that our algorithm uses Powell optimization of 2D and 3D parameters together rather than a registration of 2500 slices followed by a separate steepest gradient descent of the best one.

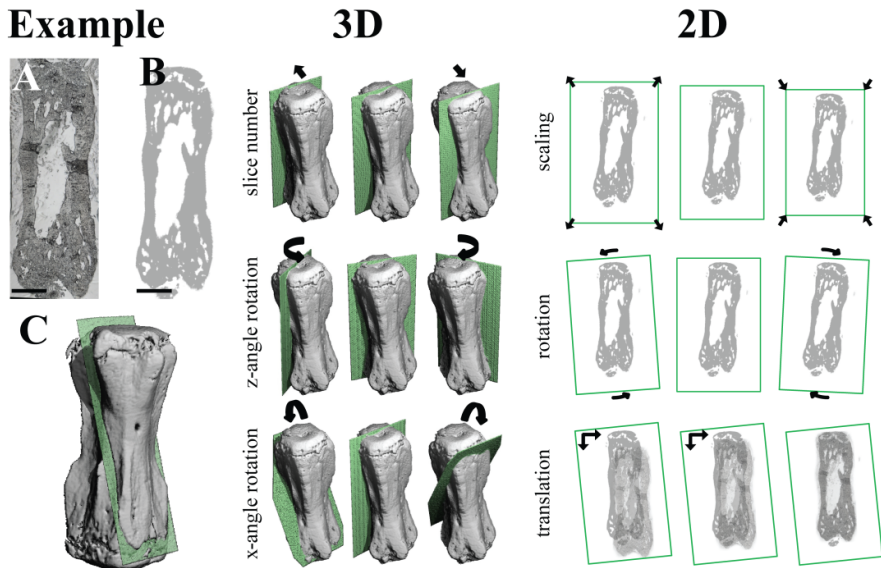


**Figure 2.3:** A graphical overview of the precursor to this project's registration algorithm [1].

## Chapter 3

---

# Materials and Methods

---

For this project, the materials required were:

- Access to the group's git server
- Access to Euler in order to generate synthetic datasets and run the registration algorithm
- Access to the group's Jupyter server on Malleus to perform data analysis and visualization

The micro-CT images used in this project were acquired at a nominal resolution of 10.5  $\mu\text{m}$  using a vivaCT40 scanner from Scanco Medical AG, Brüttisellen, Switzerland. Images were acquired *in vivo* for four mice, each with a different BV/TV i.e. bone volume over total volume. The micro-CT images were binarized for this project.

### 3.1 Generation of synthetic datasets

Synthetic histological 2D slices were virtually generated from the 3D micro-CT images. Note that the z-axis is along the longitudinal axis of the mouse femur. The synthetic 2D slices are elastically deformed as a way to simulate potential deformations that occur when a femur sample is cut by a microtome. In order to obtain the synthetic dataset for each mouse, the following steps were followed:

1. A plane is initialized at  $x = 160$  pixels i.e. in the center of the x-limits of the 3D micro-CT image.
2. The plane is rotated around the z-axis by  $\varphi$  degrees. Then, the plane is rotated around the y-axis by  $\theta$  degrees. The values of  $\varphi$  and  $\theta$  are decided prior to this.

### 3. MATERIALS AND METHODS

---

3. A bounding box along the x-axis is defined as well as the number of slices desired. The plane (oriented based on step 2) is shifted to  $N_{slices}$  equally spaced positions within the bounding box. At each of the positions, a 2D slice of the micro-CT image is sampled across the plane.  $N_{slices} = 10$  slices are sampled. The x-axis positions are called  $dx$ .
4. Each of the 10 slices are elastically deformed using a random deformation grid with a Gaussian kernel via the *elasticdeform* package on Python. [8]. The standard deviation,  $\sigma$ , is set to integer values ranging from 1 to 5. For each  $\sigma$  value, the elastic deformation is performed five times.

A complete list of parameters is as follows. Note that the parameters that are adjusted as part of the synthetic dataset are bold and underlined:

- $\underline{\varphi}$ : Rotation angle about the z-axis
- $\underline{\theta}$ : Rotation angle about the y-axis
- $\psi$ : Rotation angle about the x-axis. This is set to 0.
- $\underline{dx}$ : The displacement of the sampling plane along the x-axis.
- $dy$ : The displacement of the sampling plane along the y-axis. This is set to 0.
- $dz$ : The displacement of the sampling plane along the z-axis. This is set to 0.
- $k_x$ : The scaling factor of the 2D slice along the x-direction of the slice. This is set to 0.
- $k_y$ : The scaling factor of the 2D slice along the y-direction of the slice. This is set to 0.

The synthetic dataset was generated by running bash scripts on the Euler cluster that executed Python scripts. These scripts executed three times for each mouse, resulting in three synthetic datasets per mouse. For each of the three times,  $\varphi$  and  $\theta$  are randomly sampled from a predefined range of values.

## 3.2 Registration algorithm

The registration algorithm begins with a plane that will sample the micro-CT 3D image. The sampled image is then registered in 2D to the synthetic histological slices. The 8 parameters listed above are tuned depending on the cost function(s) being used.  $k_x$  and  $k_y$  are the affine parameters in 2D and the rest are rigid body transformations in 3D. The goal is to find the optimal

parameters that achieve the best registration, and the overall process is as follows:

1. The initial plane is determined by an initial guess for translation and rotation (outlined in Subsection 3.2.1) relative to the ground truth which is known.
2. Powell optimization is performed to find the optimal parameters. This optimization uses the cost function(s) outlined in Section 2.2. Steps 2 and 3 occur in conjunction with one another. The steps outline the sequence of geometric transformations. First, For each set of the parameters except  $k_x$  and  $k_y$  being evaluated, the respective plane is used to sample a 2D slice from the micro-CT image.
3. This 2D slice is then registered to the chosen synthetic slice using an affine transformation. More specifically, anisotropic scaling is applied using  $k_x$  and  $k_y$ . The cost function calculated here is used for the Powell optimizer in step 2. Along each direction that the Powell optimizer samples in the parameter space, the 2D cost function is what needs to be minimized. Note that  $k_x$  and  $k_y$  are constrained to [0.8, 1.2] i.e. their optimal value cannot deviate from the ground truth by more than 20%.

### 3.2.1 Initial guess

The initial guesses for the plane at step 1 of the registration have two aspects: translation and rotation. They are also defined by percentages ( $P_t$  and  $P_r$ ) that go from 0% to 100% in increments of 25%. For translation, the initial guess for the center of the plane is  $P_t\%$  of  $dx_{gt}$  (the ground truth  $dx$  value). For rotation, the initial guesses for  $\varphi$  and  $\theta$  are  $P_r\%$  of their respective ground truth angular values  $\varphi_{gt}$  and  $\theta_{gt}$ . Image registration was performed for all combinations of  $P_t$  and  $P_r$ .

### 3.2.2 Cost functions

The four cost functions used were EDTPe, EDTnMI, nMI and DS (Section 2.2). These functions were applied to fine tune the affine transformation parameters in step 3 of the registration algorithm above, and their values were used in the Powell optimizer in step 2. Not only was each cost function applied on its own, but all possible combinations of these functions (2, 3 and all the functions) were also applied. The combinations summed the cost functions. These combinations were calculated in order to evaluate whether combining cost functions may yield better registration accuracies and speeds than the lone cost functions.

The number of iterations of the Powell optimizer was capped at 50 i.e. after 50 iterations the optimizer would terminate regardless of whether the de-

### **3. MATERIALS AND METHODS**

---

sired accuracy was reached. A cap of 24 hours was also set on the duration of the optimization.

After the optimizer terminated, its results would be stored in a CSV file. This file contained the ground truth and optimized values for the 8 parameters in Section 3.1. It also contained:

- Number of iterations
- Total runtime
- Convergence metric which was calculated from the cost functions
- Statistics pertaining to the dense registration error (DRE). The DRE is the Euclidean distance between a registered pixel and its respective ground truth position [9]. This was calculated for every pixel in the registered image and then statistics including the median, mean, interquartile range and 95th percentile were stored.

All data analysis was conducted on Python via the group's Jupyter server. The CSV files from each run were read using *pandas*, analysis was conducted with *numpy* and data visualization was done with *matplotlib*. I wrote my own module to retrieve, analyze and plot data using these libraries.

## Chapter 4

---

# Results and Discussion

---

### 4.1 Generation of synthetic slices

Slices were generated as per Section 3.1. Upon comparing the left and right sided images in Figs. 4.1, 4.2, 4.3 and 4.4, we can see that slices were successfully sampled and deformed. The area of the bone tissue as a fraction of the total volume is as expected as we go through the same figures keeping BV/TV in mind.

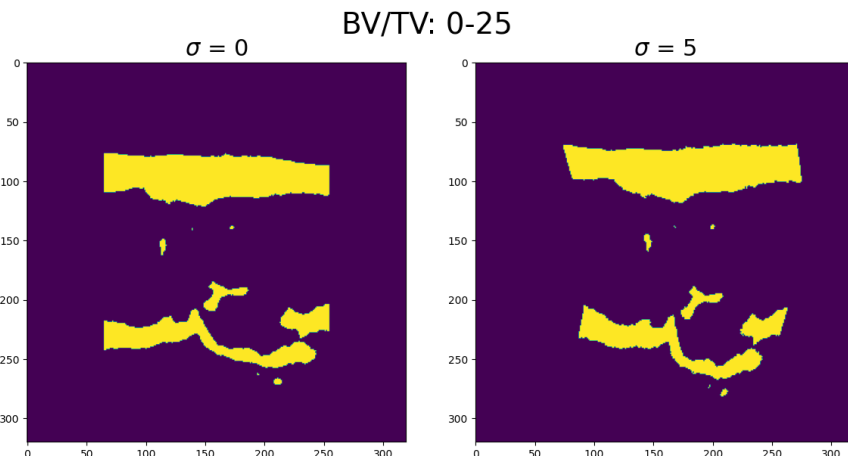


**Figure 4.1:** Synthetic 2D slices for  $BV/TV = 0.25$ . Left: no deformation. Right: maximum deformation ( $\sigma = 5$ )

#### 4. RESULTS AND DISCUSSION

---

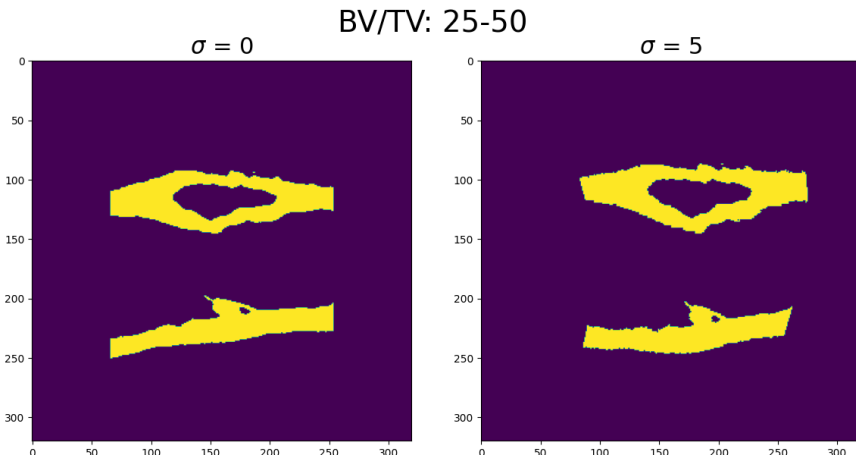


**Figure 4.2:** Synthetic 2D slices for  $\text{BV}/\text{TV} = 25-50$ . Left: no deformation. Right: maximum deformation ( $\sigma = 5$ )

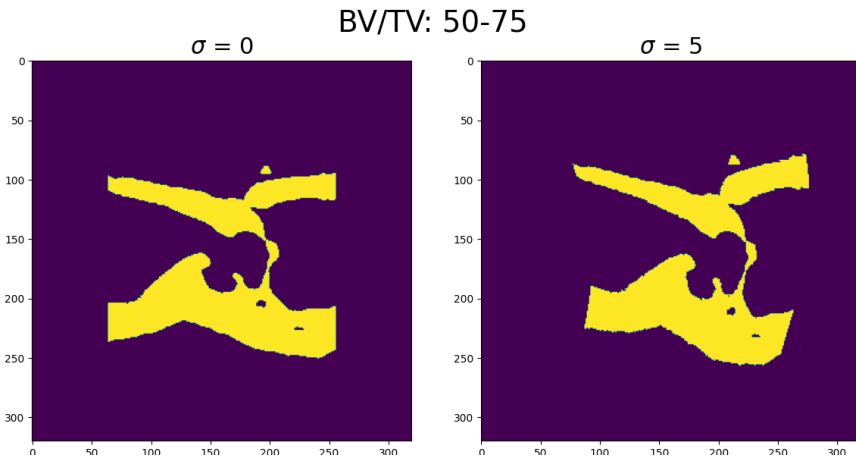


**Figure 4.3:** Synthetic 2D slices for  $\text{BV}/\text{TV} = 50-75$ . Left: no deformation. Right: maximum deformation ( $\sigma = 5$ )

## 4.2. Evaluation of initialization and deformation on registration results

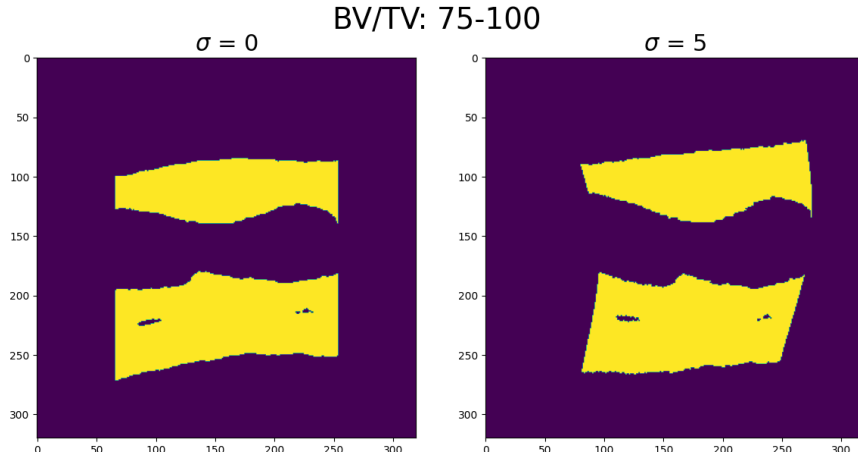


**Figure 4.4:** Synthetic 2D slices for  $BV/TV = 75-100$ . Left: no deformation. Right: maximum deformation ( $\sigma = 5$ )

## 4.2 Evaluation of initialization and deformation on registration results

The goal of this section was to evaluate how initialization and the degree of deformation  $\sigma$  would affect how the algorithm ran.

### 4.2.1 Successful convergence of the Powell optimizer

A run was considered to have converged if the number of iterations was less than 50. This meant that the accuracy desired from the Powell optimizer was reached before the process was hard coded to stop.

For each mouse with differing  $BV/TV$ , I found the combination of cost functions (Section 2.2) that achieved the highest percentage of converged runs. This was done for each initialized translation and rotation as well as for each degradation level  $\sigma$ . Recall that each mouse had three associated datasets. I found the aforementioned cost functions for each dataset and then selected the maximum from those. This was possible as each dataset is independent from the others.

I expected two results:

- $R_\sigma$  : the percentage of converged runs would get lower as  $\sigma$  increased. It should be more difficult to register a slice from the micro-CT image to a highly deformed synthetic slice and therefore it would take more iterations to meet the termination criterion for the Powell optimizer.
- $R_i$  : the percentage of converged runs would be highest for initializations that are closest to the ground truth i.e. for high initialization percentage values. If the initialization is close to the ground truth, then

#### 4. RESULTS AND DISCUSSION

---

the starting point for the Powell optimizer would already have a low cost function value. This should result in a higher likelihood of convergence before 50 iterations.

**BV/TV: 0-25, (Fig. 4.5):**  $R_\sigma$  was valid as greater  $\sigma$  values have a lower percentage of converged runs.  $R_i$  was also valid as in each grid, the percentage of converged runs increases as both the rotation and translation percentage increase. This effect is clearer for the rotation initialization. The bottom two plots in the figure illustrate this. For  $\sigma = 1$ , the convergence rate goes from 0.3% to 100% as the rotation initialization increases with a fixed translation initialization. This rate goes from 81.3% to 100% for translation initialization with a fixed rotation initialization. This also indicates that for low BV/TVs, the rotation initialization plays a stronger role than translation in the success of the registration. This claim is also supported by the fact that for a 0% rotation initialization, the convergence percentages are very low (the maximum is 0.5% for all  $\sigma$ ) regardless of the translation. This initialization corresponds to the point furthest away from the ground truth rotation parameters. The same cannot be said for the translation initialization as the convergence percentages are as high as 81.3% for a translation initialization of 0%. In general, for the lowest BV/TV values, optimization combinations that contain either nMI or EDTnMI perform best.

**BV/TV: 25-50, (Fig. 4.6):**  $R_\sigma$  and  $R_i$  were valid. For all 6 subplots, optimization combinations that include EDTnMI or nMI generally perform the best; the majority of best combinations include one of these. EDTnMI is the more frequently appearing of the two. There are a lot of incidences of solely EDTnMI yielding the best convergence percentage, especially for mid-to-high initialization percentages (50% and above). For high levels of deformation ( $\sigma \geq 6$ ), EDTPe features in combinations that yield the highest convergence percentage. However, this percentage is still much lower than for low  $\sigma$ .

**BV/TV: 50-75, (Fig. 4.7):**  $R_\sigma$  and  $R_i$  were valid. Similar to lower BV/TVs, regardless of  $\sigma$ , combinations including EDTnMI or nMI perform the best as these are part of the majority of the best combinations. In general compared to the lower BV/TV values, EDTPe is more prominent as part of combinations that achieve the most converged runs, especially at higher initializations.

**BV/TV: 75-100, (Fig. 4.8):**  $R_\sigma$  and  $R_i$  were valid. For high translation initializations, combinations containing EDTPe perform the best. This is more prominent than lower BV/TVs. For low translation and rotation initializations, combinations with nMI or EDTnMI perform the best.

## 4.2. Evaluation of initialization and deformation on registration results

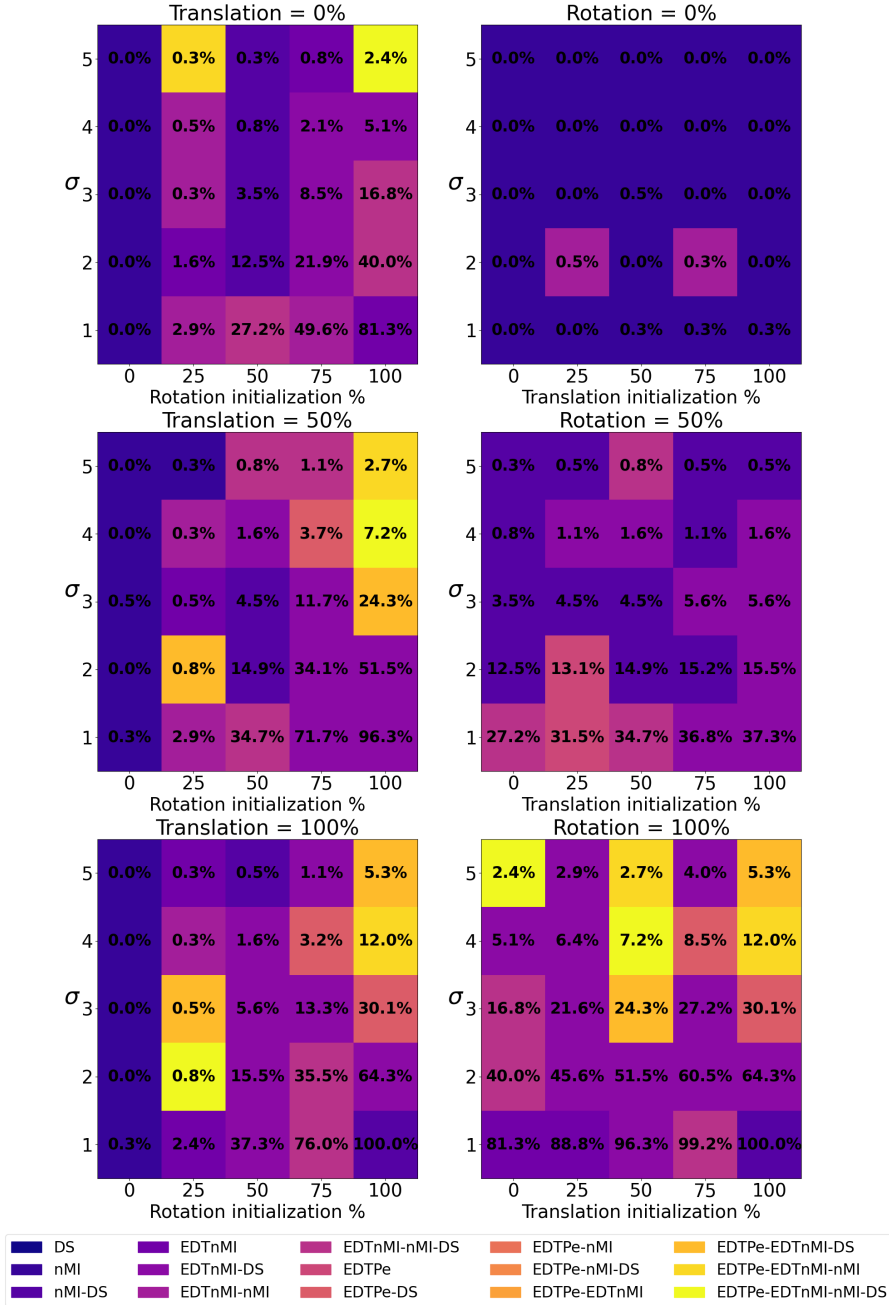


**Figure 4.5:** BV/TV: 0-25. The entries in each box in the subplots are the percentage of runs that converged. The colours correspond to the best combination of cost functions.

## 4. RESULTS AND DISCUSSION



**Figure 4.6:** BV/TV: 25-50. The entries in each box in the subplots are the percentage of runs that converged. The colours correspond to the best combination of cost functions.

## 4.2. Evaluation of initialization and deformation on registration results

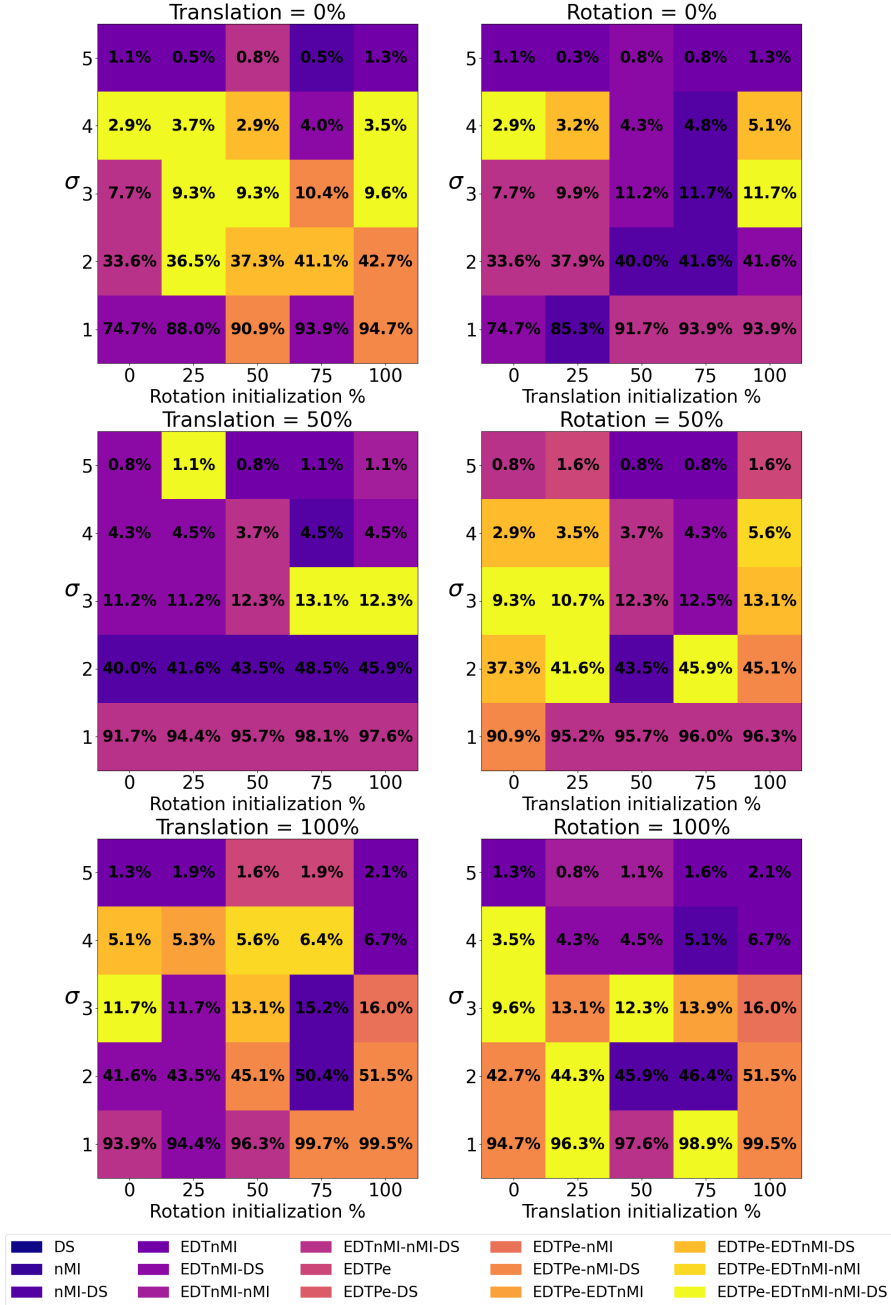


**Figure 4.7:** BV/TV: 50-75. The entries in each box in the subplots are the percentage of runs that converged. The colours correspond to the best combination of cost functions.

#### 4. RESULTS AND DISCUSSION

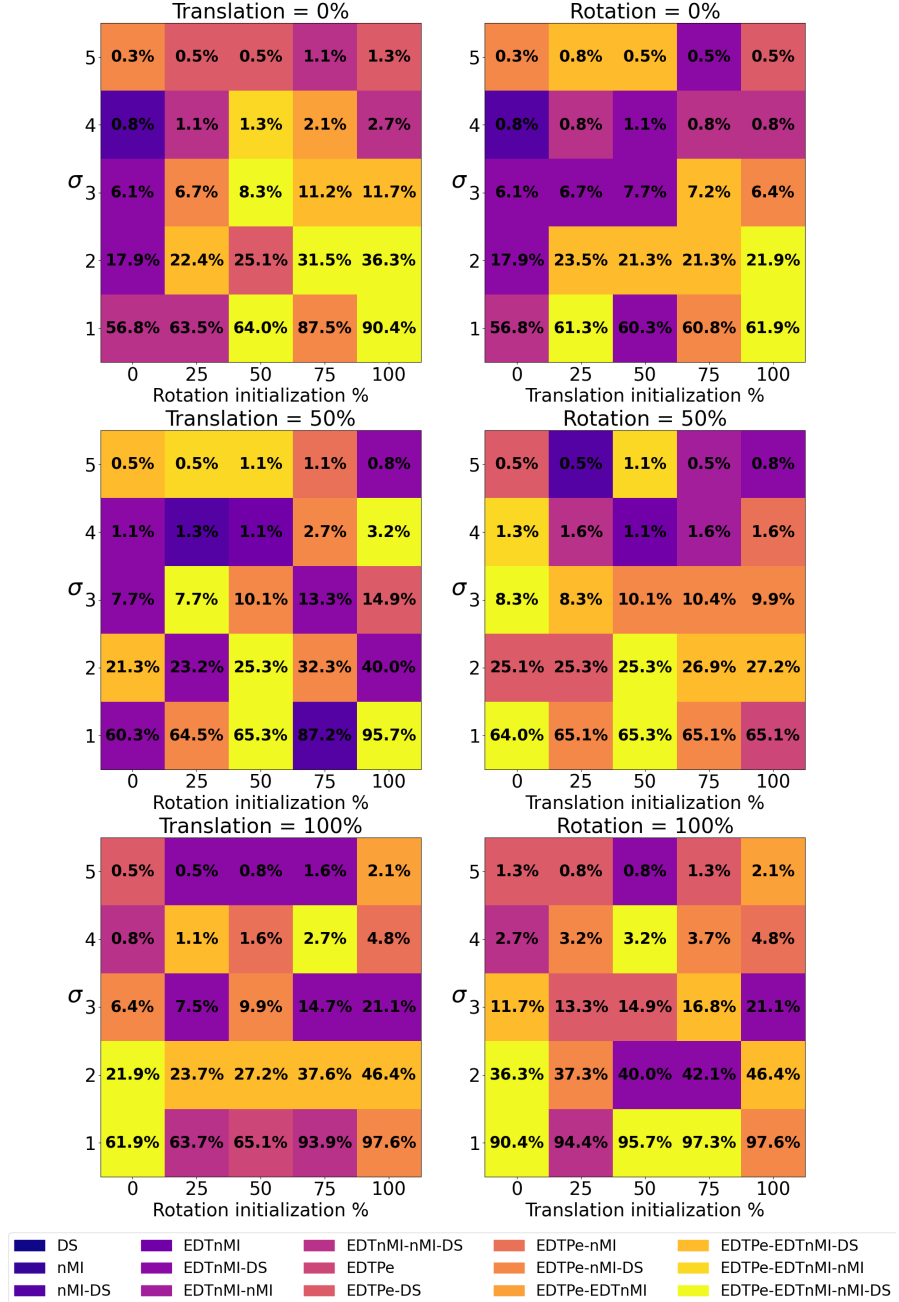


**Figure 4.8:** BV/TV: 75-100. The entries in each box in the subplots are the percentage of runs that converged. The colours correspond to the best combination of cost functions.

**Overall observations:** For higher BV/TV values (Figs. 4.7 and 4.8), combinations with EDTPe perform better with regards to the number of runs that converge. For lower BV/TVs (Figs. 4.5, 4.6), combinations containing nMI

---

## 4.2. Evaluation of initialization and deformation on registration results

---

or EDTnMI are the best for registration. This however applies to all BV/TVs in general. If one wanted to reduce the number of cost functions being used, these two are the best candidates to select.

For all the mice, combinations containing two cost functions or less are best for the majority of initializations and deformations. This means that the complexity of calculating three or more cost functions may be avoided in the future, thereby speeding up computations.

$R_\sigma$  and  $R_i$  were valid for all the mice. For high BV/TV mice with low  $\sigma$ , the initializations didn't have a strong effect on the convergence percentage. However for the same mice but with higher  $\sigma$ , the effects of the initialization followed  $R_i$ . If one were to inspect any of the subplots, they would observe that the variation along the vertical axis is greater than that along the horizontal axis. This indicates that the deformation  $\sigma$  plays a bigger role than the initializations in whether or not the registration converges.

### 4.2.2 Accuracy of the Powell optimizer

In order to evaluate the registration accuracy, I examined the dense registration error (DRE, outlined in Section 3.2). I wanted to see the effects of deformation, initialization and BV/TV on DRE. The DRE used for this purpose is stored in the runs' CSV files as the masked DRE. This means that the DRE is calculated over the pixels of the binary image that correspond to bone tissue.

I expected:

- $R_\sigma$  : the DRE should increase as deformation increases. It should be more difficult to register a slice from the micro-CT image to a highly deformed synthetic slice and so the error should be greater.
- $R_i$  : the DRE should be lowest for initializations that are closest to the ground truth i.e. for high initialization percentage values. If the initialization is close to the ground truth, then the starting point for the Powell optimizer would already have a low cost function value, resulting in a lower error.

**BV/TV: 0-25, (Fig. 4.9):**  $R_i$  and  $R_\sigma$  were valid.  $\sigma$  affected the DRE as expected but not as strongly as initialization. For low translation and rotation initializations ( $\leq 25\%$ ), EDTPe was a part of the majority of best cost function combinations and was a part of all the best combinations for  $\sigma \geq 3$ . For all deformation values, either EDTnMI or nMI were a part of the best cost function combinations for the majority of initializations. Judging by the bottom two subplots, rotation is more impactful than translation for the initialization. For the same initializations (100%), the subplot for rotation ini-

#### 4. RESULTS AND DISCUSSION

---

tialization of 100% had distinctly lower DREs than a translation initialization of 100%.

**BV/TV: 25-50, (Fig. 4.10):**  $R_i$  and  $R_\sigma$  were valid.  $\sigma$  affected the DRE as expected but not as strongly as initialization. For high initializations ( $\geq 75\%$ ) of both translation and rotation, DS appears in the majority of the best cost function combinations. In general, EDTnMI and nMI are present in the majority of the best combinations. One of those two is always present for low initializations ( $\leq 50\%$ ). Similarly to a BV/TV of 0-25, the rotation initialization has a stronger effect than translation.

**BV/TV: 50-75, (Fig. 4.11):**  $R_i$  and  $R_\sigma$  were valid.  $\sigma$  affected the DRE as expected but not as strongly as initialization. Rotation was again the more impactful of the initializable parameters. For high deformation levels and initializations (especially rotation), EDTPe was present in the majority of cost function combinations. In general, one of EDTnMI and nMI were present in every single cost function combination.

**BV/TV: 75-100, (Fig. 4.12):**  $R_i$  and  $R_\sigma$  were valid.  $\sigma$  affected the DRE as expected but not as strongly as initialization. Rotation was again the more impactful of the initializable parameters. For high translation initializations, EDTPe as part of cost function combinations was very prominent. For low initializations of translation and rotation, EDTnMI or nMI were present in every cost function combination.

## 4.2. Evaluation of initialization and deformation on registration results

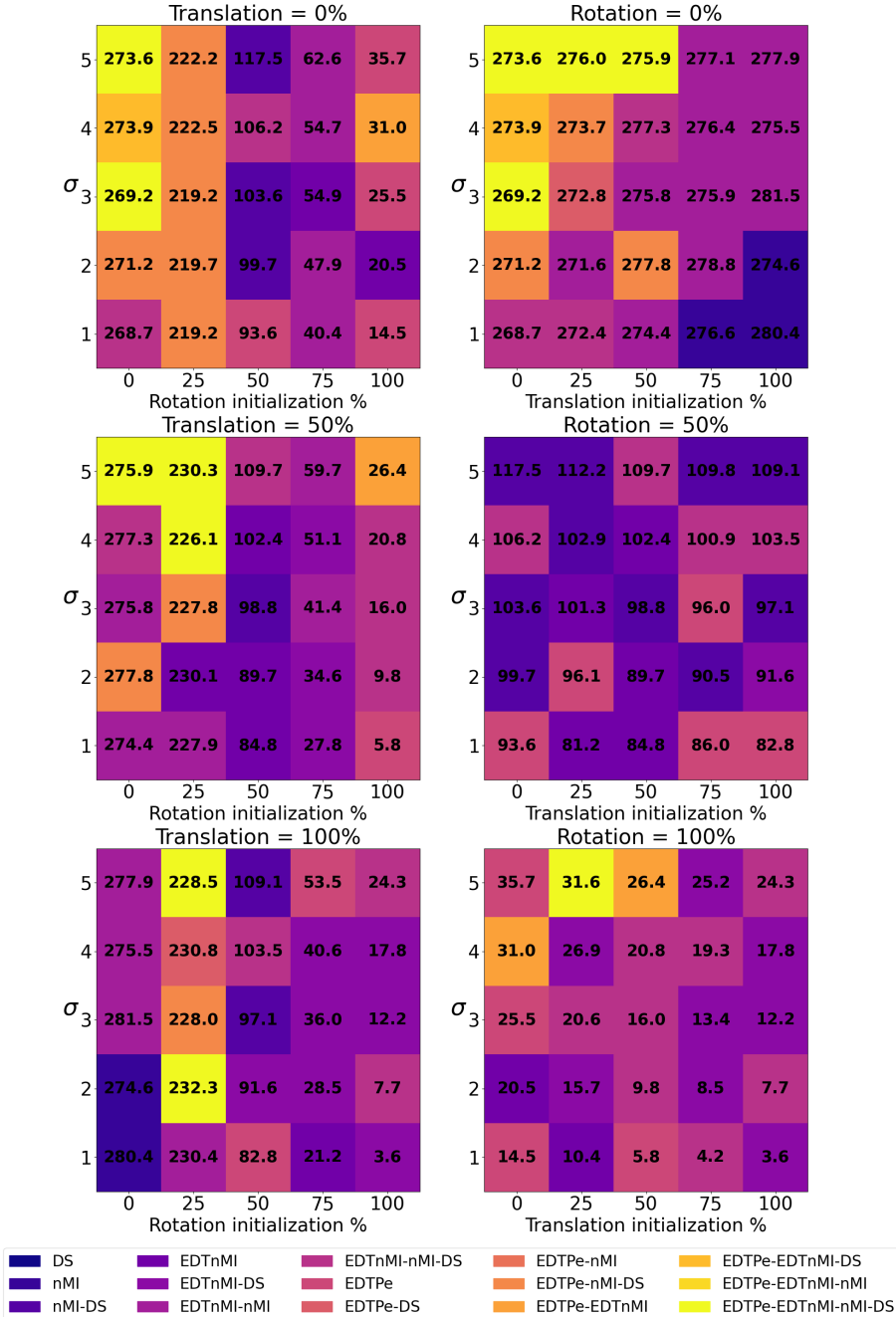


**Figure 4.9:** BV/Tv: 0-25. The entries in each box in the subplots are the best mean masked DRE for the respective initialization and  $\sigma$ . The colours correspond to the best combination of cost functions.

## 4. RESULTS AND DISCUSSION

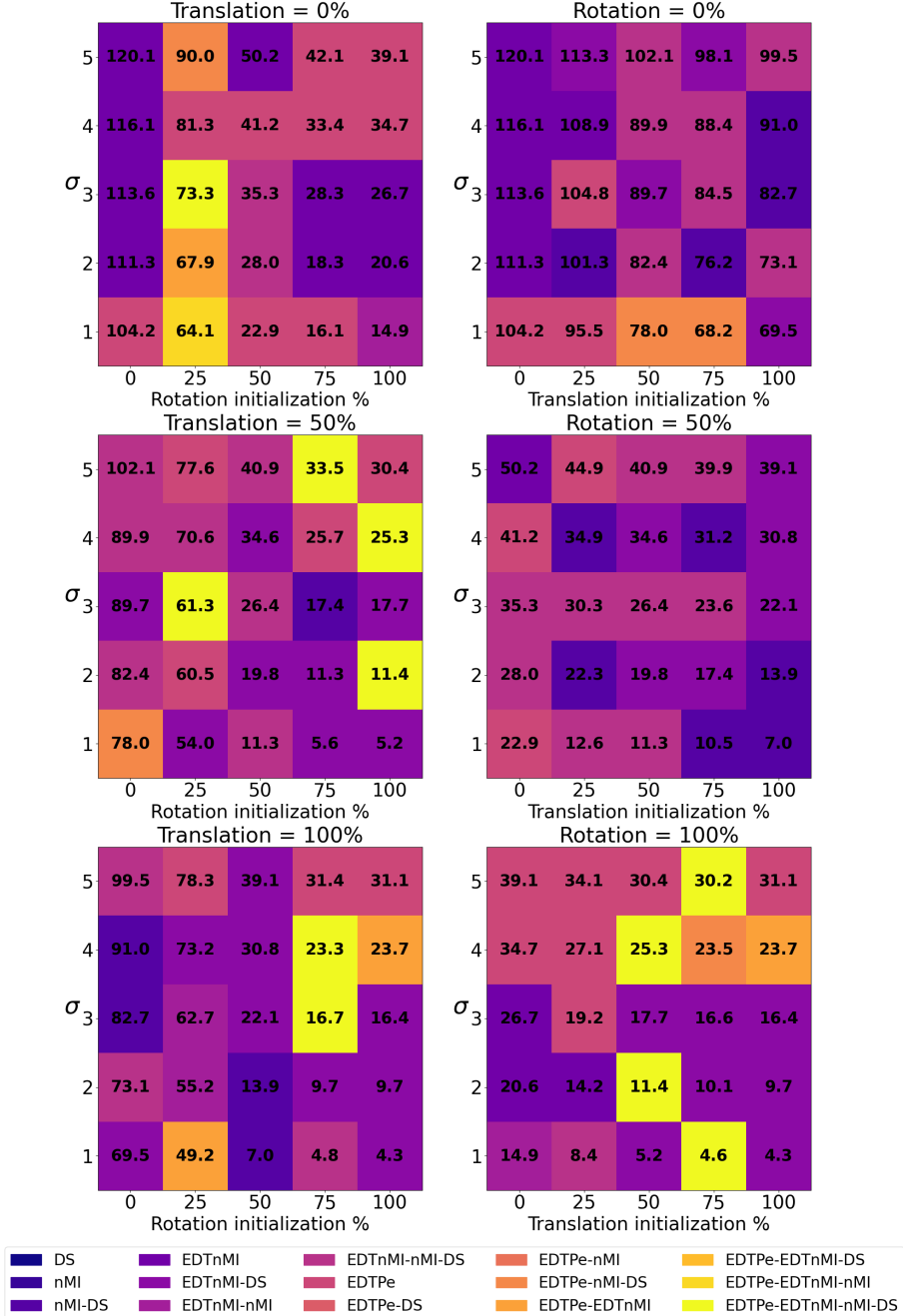


**Figure 4.10:** BV/TV: 25-50. The entries in each box in the subplots are the best mean masked DRE for the respective initialization and  $\sigma$ . The colours correspond to the best combination of cost functions.

## 4.2. Evaluation of initialization and deformation on registration results

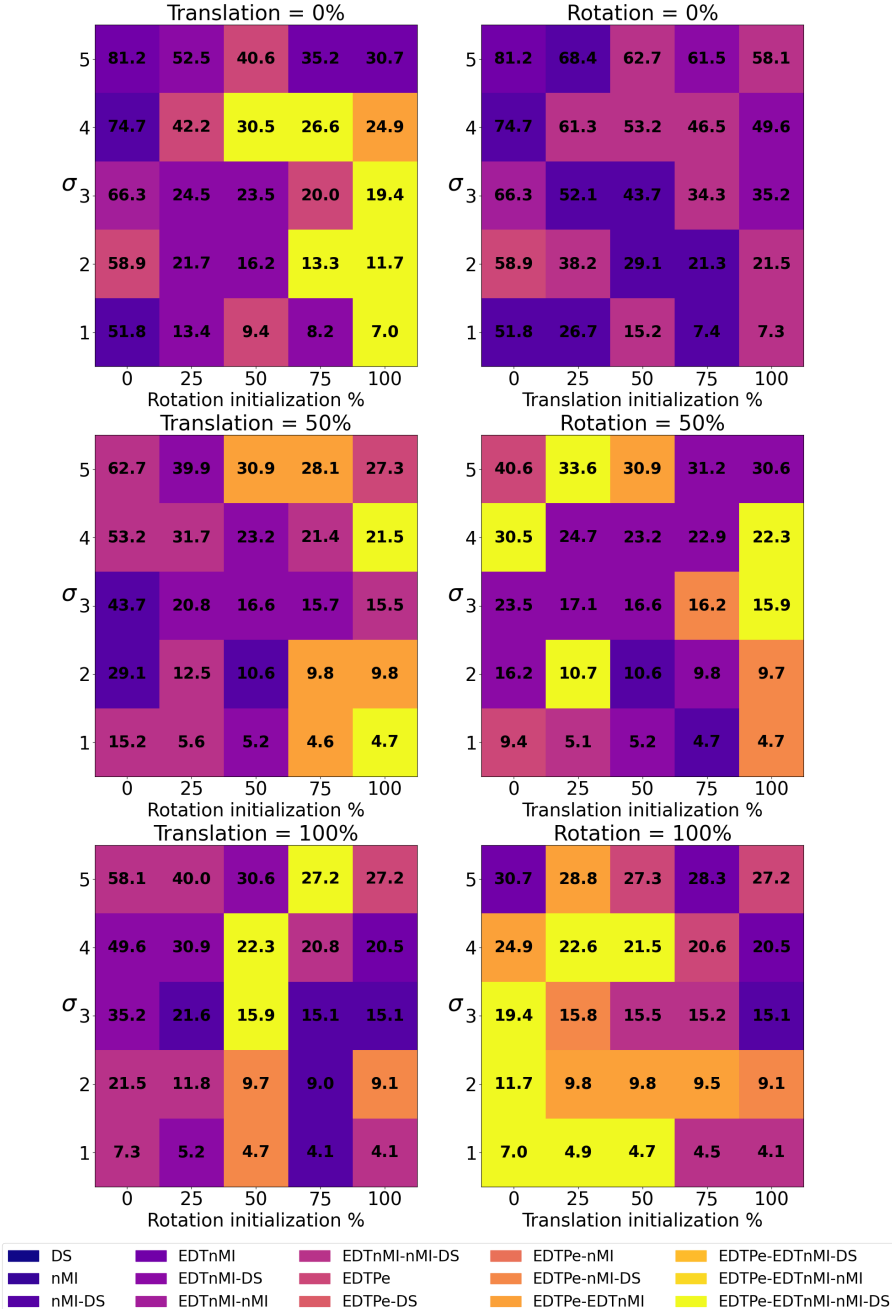


**Figure 4.11:** BV/TV: 50-75. The entries in each box in the subplots are the best mean masked DRE for the respective initialization and  $\sigma$ . The colours correspond to the best combination of cost functions.

#### 4. RESULTS AND DISCUSSION

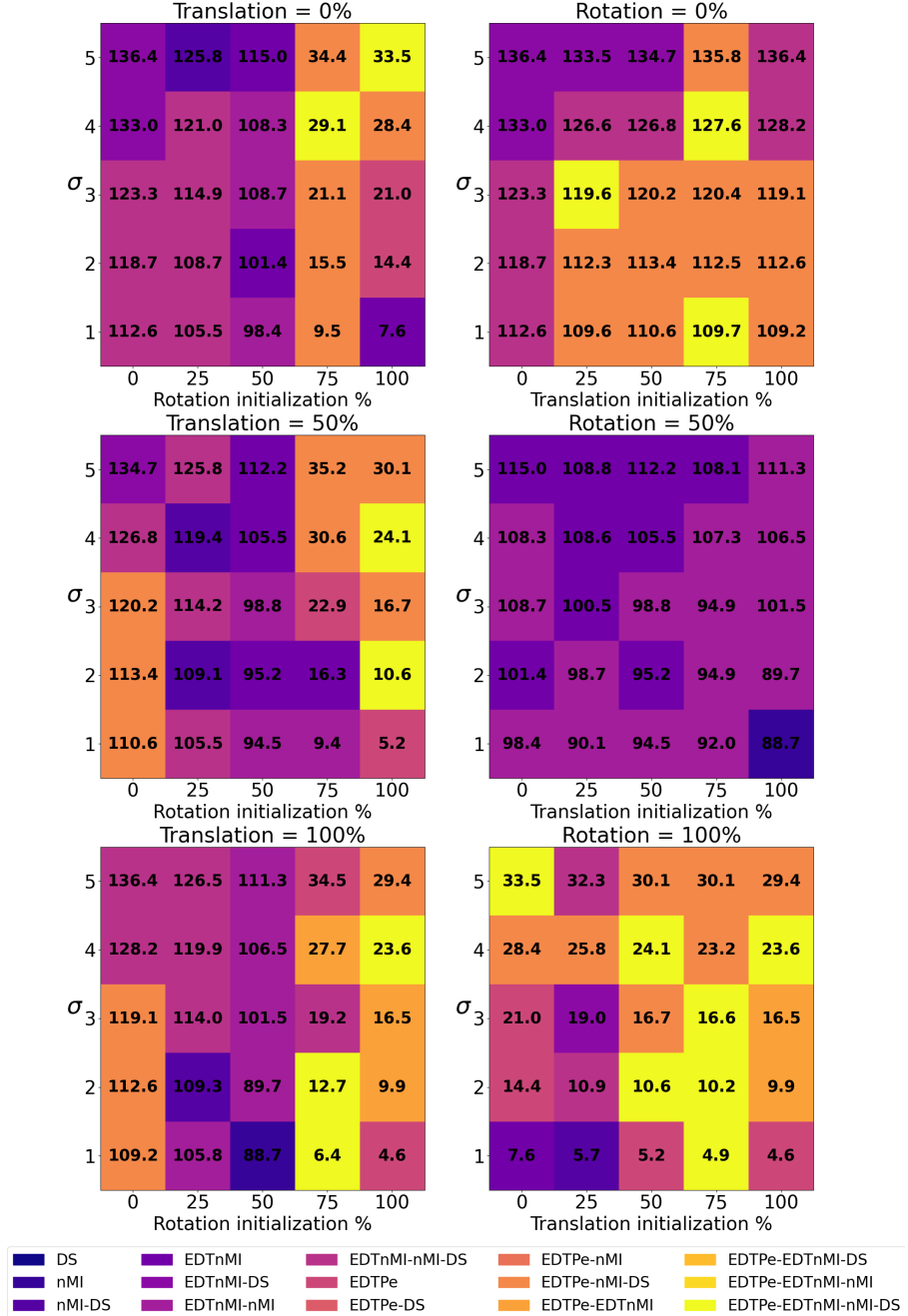


**Figure 4.12:** BV/TV: 75-100. The entries in each box in the subplots are the best mean masked DRE for the respective initialization and  $\sigma$ . The colours correspond to the best combination of cost functions.

**Overall observations:** My expected results did occur. Unlike in Section 4.2.1, the initializations were more impactful than  $\sigma$  in affecting the variable

---

## 4.2. Evaluation of initialization and deformation on registration results

---

of interest, which was DRE in this case. Again, EDTnMI and nMI were the most prominent cost functions. For initializations close to the ground truth for mice with high BV/TVs, these two cost metrics can be combined with EDTPe. However, for a wider range of cases, EDTnMI and MI are the best candidates to use if the goal is to minimize the number of cost functions being used. The scale of the mean DRE values was affected by BV/TV. The higher the BV/TV, the lower the general DRE value.

### 4.2.3 Effect of displacement $|dx_{gt}|$ on DRE

I wanted to investigate whether the position of the sampling plane in 3D affected the registration. We can imagine a bone as a cylinder with the z-axis along the long axis. We initialize a plane at the central x value and rotate it around the z-axis followed by around the y-axis. Then the plane is translated along the x-axis. For x positions that are far from the center, the plane will intersect with the wall of the bone. When the 3D image is sampled along this plane, there will be a loss of information from the sample. I expected this to cause an increase in the mean DRE for high displacements  $dx$ . Because there are fewer pixels that correspond to tissue, the DRE from the tissue pixels would have a higher standard deviation compared to a slice taken from a plane that was closer to the center of the x-bounds.

First, I plotted the mean DRE as a function of the displacement of the sampling plane from the center along x (ground truth of  $dx$  or  $dx_{gt}$ ). This is visible in Fig. 4.13. This plot was generated from the mouse with the highest BV/TV of 75-100. This is as the aforementioned loss of information would be greater for a sample with a higher number of bone tissue pixels. Looking at Fig. 4.13, the relationship between the displacement  $dx_{gt}$  and the mean DRE appears to be random for all cost function combinations. The standard deviation of does not increase with the displacement either. This may be because this plot was made for all deformations; the deformation levels were not separated.

For the four cost functions, used individually for registration, I plotted the displacement vs mean DRE for each deformation level. These plots were generated from the same dataset as Fig. 4.13. I expected to see a greater DRE and uncertainty for higher  $\sigma$  values. I also expected to see the DRE increase with  $dx_{gt}$ .

Again, the relationship of the displacement  $dx_{gt}$  with the mean DRE was random (Figs. 4.14-4.17). These variables did not correlate as expected. Furthermore,  $\sigma$  did not seem to affect the mean DRE, as all the lines in each plot are close together, rather than being offset from each other. This was the case for all the cost functions.

I made plots similar to those from Figs 4.13-4.17 for mice with different

#### 4. RESULTS AND DISCUSSION

---

BV/TVs and observed the same trends as detailed above. The displacement has no effect on the DRE of the registration. This is because even though the synthetic slices sampled with high displacements had some lost data, the registration algorithm would also sample slices with similarly lost data. The sampled slice and synthetic slice would then be registered no differently than before. Additionally, for each displacement, the deformation does not have an effect either.

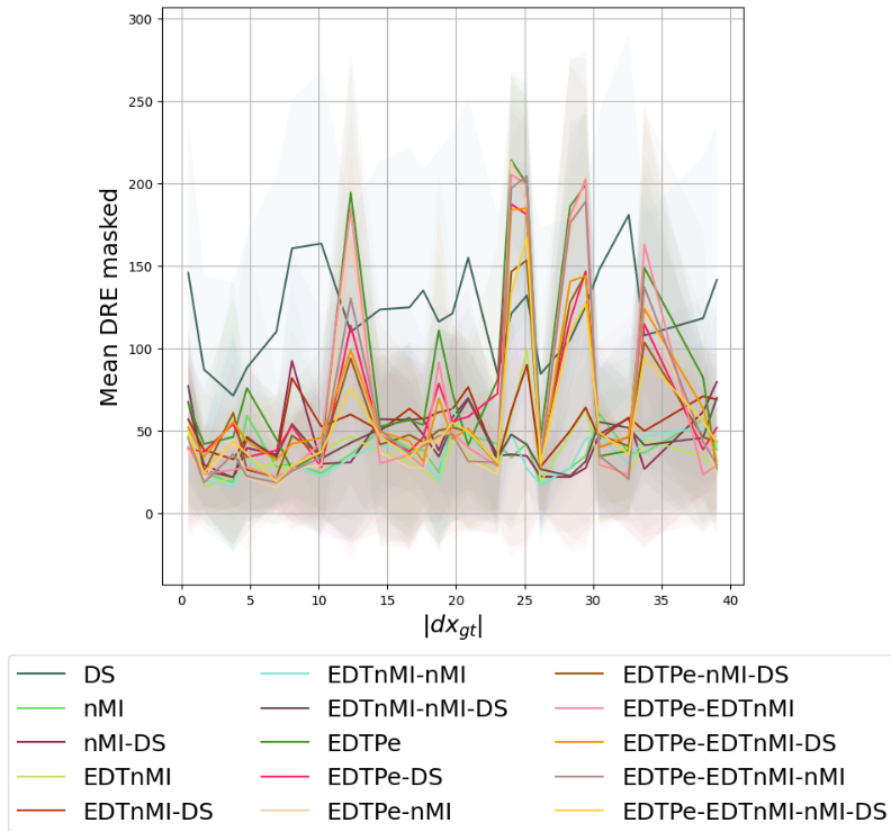


**Figure 4.13:** A plot of the displacement vs the mean masked DRE, calculated for a BV/TV of 75-100. The lines were made for all the possible cost function combinations.

## 4.2. Evaluation of initialization and deformation on registration results

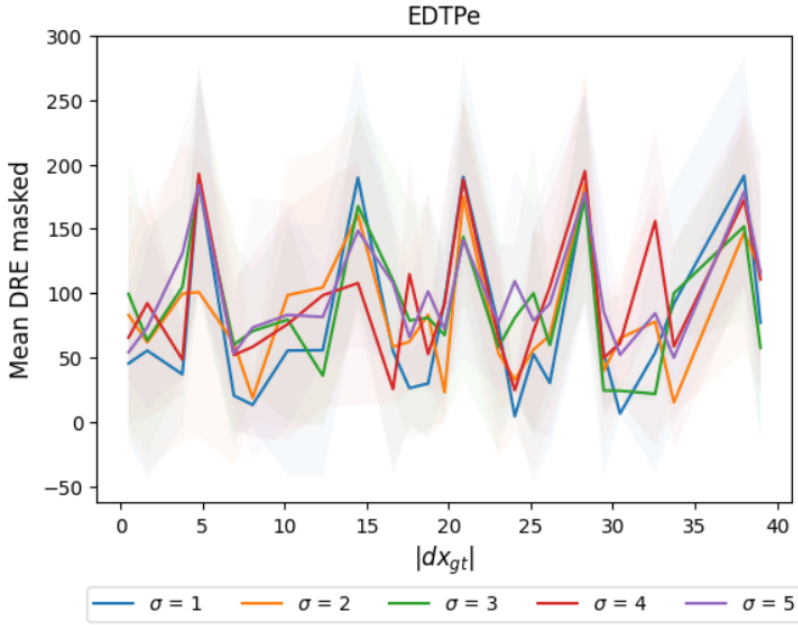


**Figure 4.14:** A plot of the displacement vs the mean masked DRE, calculated for a BV/TV of 75-100. The lines were made for all the deformation levels. The cost function for this plot was EDTPe.

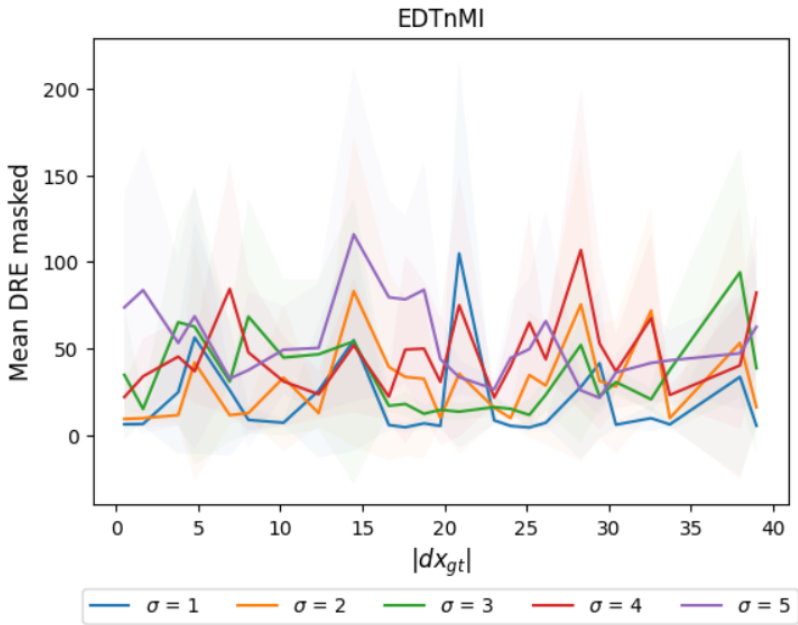


**Figure 4.15:** A plot of the displacement vs the mean masked DRE, calculated for a BV/TV of 75-100. The lines were made for all the deformation levels. The cost function for this plot was EDTnMI.

#### 4. RESULTS AND DISCUSSION

---

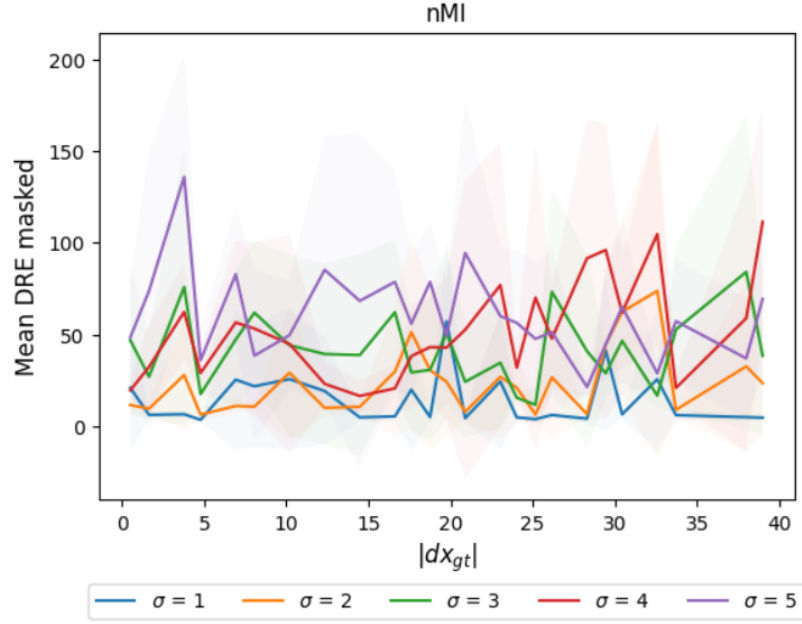


**Figure 4.16:** A plot of the displacement vs the mean masked DRE, calculated for a BV/TV of 75-100. The lines were made for all the deformation levels. The cost function for this plot was nml.

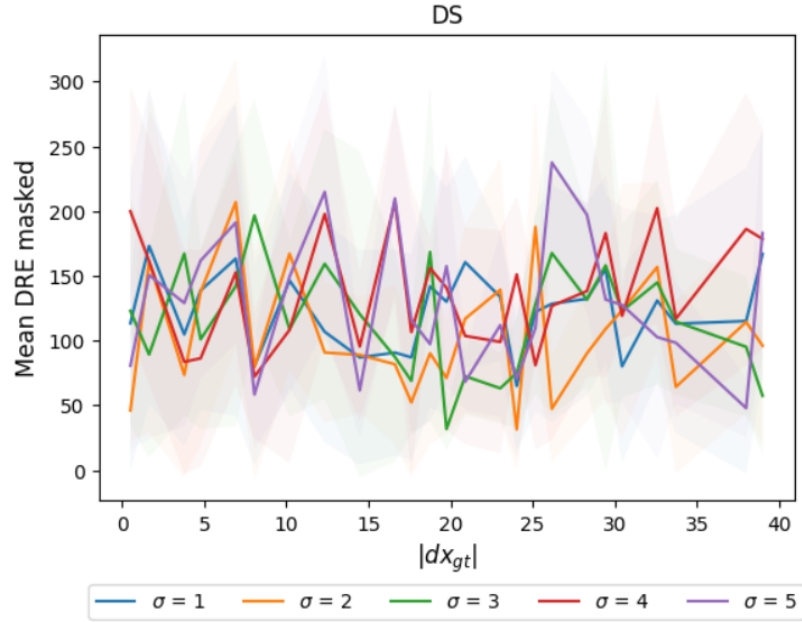


**Figure 4.17:** A plot of the displacement vs the mean masked DRE, calculated for a BV/TV of 75-100. The lines were made for all the deformation levels. The cost function for this plot was DS.

## Chapter 5

---

# Conclusion

---

This project took me on a journey through the aspects of evaluating an image registration pipeline. From 3D micro-CT images of mouse femurs, I generated synthetic 2D slices and elastically deformed them in order to simulate the bone sectioning process done via a microtome. Because this sectioning is done so that histological sections may be acquired, there needs to be a way to register the 2D histological images to its bone's respective 3D micro-CT image. I then executed a script to perform 2D-3D registration via Powell optimization.

In order to simulate the user providing an initial guess as to how the plane that was used to sample a 2D slice was oriented with respect to the micro-CT image, I carried out the registration for different initialized translational and rotational parameters. As the goal was to evaluate the effects of these initializations as well as of deformations, I analyzed and visualized the data in order to gain a deeper understanding of the mechanisms of the registration.

I found that high deformations prevented the registration algorithm from converging, which meant lower registration accuracies as the termination criterion of the Powell optimizer could not be met. The deformation was the most significant factor in whether or not the algorithm converged, as positional initializations far from the ground truth still achieved a high percentage of convergence for low amounts of deformation. One way to increase the amount of converging runs for a high degree of deformation could be to remove the upper bound on number of iterations. However, this would result in the registration taking a lot longer to complete. Initializing the translation and rotation parameters such that the sampling plane was far away from the ground truth also resulted in fewer runs converging. I found that rotation had a greater impact than translation, though they both followed the same trend. Similarly, I found that for the dense registration error (DRE) to be lowest, the initializations should be close to the ground truth and the degree of deformation should be low. Again, rotational initialization

## 5. CONCLUSION

---

was more significant in effecting the DRE than translational initialization.

The cost functions EDTnMI (Euclidean distance transformed normalized mutual information) and nMI (normalized mutual information) were the best performing cost functions with regards to both convergence and the DRE. One way to minimize the complexity of the registration algorithm could be to use two or fewer cost functions. These two cost functions would be the best candidates and could help decrease registration runtimes.

I attempted to study whether 2D slices sampled away from the bone samples' centers would affect the DRE, and therefore the accuracy. I found that neither the displacement of the sampling plane from the center nor the deformation had any relationship with the DRE.

---

## Bibliography

---

- [1] A.J. Trüssel. Spatial mapping and high throughput microfluidic gene expression analysis of osteocytes in mechanically controlled bone remodeling. (22716), 2015.
- [2] A.C. Scheuren et al. Mechano-regulation of trabecular bone adaptation is controlled by the local in vivo environment and logarithmically dependent on loading frequency. *Front. Bioeng. Biotechnol*, 8(p. 1211), 2020.
- [3] Ender Konukoglu. Lectures in medical image analysis, 2022.
- [4] Pete Bankhead. Introduction to bioimage analysis, 2022.
- [5] A.C. Victorino A.M. Neto, et al. Image processing using pearson's correlation coefficient: Applications on autonomous robotics. *13th International Conference on Mobile Robots and Competitions (Robotica in Lisbon, Portugal)*, 2013.
- [6] Bayesia Lab. Mutual information.
- [7] V.S. Vasiliadis and R Conejeros. Powell method. *Encyclopaedia of Optimization*, (p. 2001-2003), 2001.
- [8] Gijs van Tulder. elasticdeform, 2018.
- [9] E.L. Lundin et al. Automatic registration of 2d histological sections to 3d microct volumes: Trabecular bone. *Bone*, 105(p. 173-183), 2017.

## Declaration of originality

The signed declaration of originality is a component of every semester paper, Bachelor's thesis, Master's thesis and any other degree paper undertaken during the course of studies, including the respective electronic versions.

Lecturers may also require a declaration of originality for other written papers compiled for their courses.

---

I hereby confirm that I am the sole author of the written work here enclosed and that I have compiled it in my own words. Parts excepted are corrections of form and content by the supervisor.

**Title of work** (in block letters):

**Authored by** (in block letters):

*For papers written by groups the names of all authors are required.*

**Name(s):**

---

---

---

---

---

**First name(s):**

---

---

---

---

---

With my signature I confirm that

- I have committed none of the forms of plagiarism described in the '[Citation etiquette](#)' information sheet.
- I have documented all methods, data and processes truthfully.
- I have not manipulated any data.
- I have mentioned all persons who were significant facilitators of the work.

I am aware that the work may be screened electronically for plagiarism.

**Place, date**

**Signature(s)**



---

---

---

---

---

*For papers written by groups the names of all authors are required. Their signatures collectively guarantee the entire content of the written paper.*